LA-UR-17-29191 (Accepted Manuscript)

Generation Process of Large-Amplitude Upper-Band Chorus Emissions Observed by Van Allen Probes

Kubota, Y.
Omura, Y.
Kletzing, C. A.
Reeves, Geoffrey D.

To be published in: Journal of Geophysical Research: Space Physics

DOI to publisher's version: 10.1029/2017JA024782

Permalink to record: http://permalink.lanl.gov/object/view?what=info:lanl-repo/lareport/LA-UR-17-29191

Generation process of large-amplitude upper band chorus emissions observed by Van Allen Probes

Yuko Kubota[1,2], Yoshiharu Omura[1], Craig Kletzing[2], and Geoff Reeves[3]

Y. Kubota, yuko_kubota@rish.kyoto-u.ac.jp

[1]Research Institute for Sustainable Humanosphere, Kyoto University, Kyoto, Japan

[2]Department of Physics and Astronomy, University of Iowa, Iowa City, IA

[3]Space Science and Applications Group, Los Alamos National Laboratory, Los Alamos, NM

This article has been accepted for publication and undergone full peer review but has not been through the copyediting, typesetting, pagination and proofreading process, which may lead to differences between this version and the Version of Record. Please cite this article as doi: 10.1002/2017JA024782

Abstract. We analyze large-amplitude upper-band chorus emissions measured near the magnetic equator by the EMFISIS (Electric and Magnetic Field Instrument Suite and Integrated Science) instrument package onboard the Van Allen Probes. In setting up the parameters of source electrons exciting the emissions based on theoretical analyses and observational results measured by the HOPE (Helium Oxygen Proton Electron) instrument, we calculate threshold and optimum amplitudes with the nonlinear wave growth theory. We find that the optimum amplitude is larger than the threshold amplitude obtained in the frequency range of the chorus emissions and that the wave amplitudes grow between the threshold and optimum amplitudes. In the frame of the wave growth process, the nonlinear growth rates are much greater than the linear growth rates.

Keypoints:

- Observations by Van Allen Probes show that the upper-band chorus emissions exist both inside and outside the plasmasphere.
- The densities and thermal velocities of electrons generating the chorus emissions are evaluated from HOPE particle data.
- Observed chorus amplitude and frequency ranges agree with the nonlinear wave growth theory.

1. Introduction

Chorus emissions with highly oblique wave normal angles have been observed by Cluster satellites [*Santolik et al.*, 2009] and Van Allen Probes [*Mourenas et al.*, 2015]. Chorus is often separated into upper-band and lower-band by a gap at half the cyclotron frequency. *Li et al.* [2011] reported that upper-band chorus waves propagate more obliquely than lower-band chorus waves based on the observational results of Time History of Events and Macroscale Interactions during Substorms (THEMIS). *Santolik et al.* [2014], on the other hand, reported that wave normals tend to be closer to the direction of geomagnetic field lines as the wave amplitude increases. According to the simulation analysis of energetic electrons interacting with chorus emissions with parallel propagation [*Omura et al.*, 2015], chorus emissions play key roles in radiation belt dynamics as an accelerator of MeV electrons, while electromagnetic ion cyclotron (EMIC) rising-tone emissions are effective in scattering of relativistic electrons into the atmosphere [*Kubota and Omura*, 2017].

Omura et al. [2008] and *Omura and Nunn* [2011] proposed a nonlinear wave growth theory explaining the growing amplitude and rising-tone frequency mechanism of chorus waves with parallel propagation. Based on an analysis of data obtained by THEMIS, *Kurita et al.* [2012] reported that chorus emissions without a gap at half the cyclotron frequency are in good agreement with the nonlinear wave growth theory. The gap can be formed because of the nonlinear damping mechanism induced by the longitudinal component of a slightly oblique whistler mode wave packet [*Omura et al.*, 2009]. Using data obtained by Geotail spacecraft, *Yagitani et al.* [2014] and *Habagishi et al.* [2014] evaluated the gap bandwidths and occurrence, respectively.

In the present study, we analyze upper-band chorus emissions and emissions with a narrow gap at half the cyclotron frequency observed by Van Allen Probes. In section 2 we describe properties of the large-amplitude chorus elements in a region close to the magnetic equator in the magnetosphere based on the data measured by the EMFISIS instrument package. In section 3 we evaluate source electron distributions using HOPE data. Assuming that the source electrons form a bi-Maxwellian distribution function, we obtain the parameters to estimate both linear and nonlinear growth rates. In section 4, we compare the emissions observed by EMFISIS with the results obtained by the theoretical analyses. We present a summary and discussion in section 5.

2. EMFISIS Observational Results

Analyzing the data obtained by the EMFISIS instrument package onboard the Van Allen Probe-A, we study large-amplitude chorus emissions excited near the equator in the magnetosphere [*Kletzing et al.*, 2013]. We have performed a survey of the EMFISIS data over one month (January 2013) and found 5 cases of upper-band chorus emissions with the magnetic power spectral density greater than $10^{-7}\,\mathrm{nT}^2/\mathrm{Hz}$. These large amplitude chorus emissions are characterized by high coherence, right-hand polarization, and rising-tone frequency. As targets of case studies, we choose three different groups of the chorus emissions shown in Figure 1. The solar wind speed for each of the three cases is within a normal range of 380-420 km/s. Figure 1a shows the sum of the power spectral densities of two components of the wave magnetic field normal to the geomagnetic field $\boldsymbol{B_0}$. The white dashed lines show half the local electron cyclotron frequency f_c. The emissions consist respectively of the upper-band chorus only (Case 1), both the upper-band chorus with large amplitudes and the lower-band chorus (Case 2), and both large amplitude

upper- and lower- band chorus emissions (Case 3). The emissions in Cases 2 and 3 are separated at half the cyclotron frequency. Detailed analyses of the wave normal angle θ and the Poynting vector angle θ_s with respect to the geomagnetic field $\boldsymbol{B_0}$ are shown in Figures 1b and 1c, respectively. These wave properties are plotted only when the magnetic power spectral density shown in Figure 1a and the degree of polarization are greater than $10^{-7}\,\mathrm{nT^2/Hz}$ and 0.7, respectively. Using (17) of *Samson and Olson* [1980], we calculate the degree of polarization. As shown in Figure 1b, the emissions in Cases 1 and 2 propagate quasi-parallel to the geomagnetic field lines. The emissions in Case 3, on the other hand, propagate obliquely ($\theta \sim 45°$). From Figure 1c and magnetic latitudes (Mlat) as listed on top of Figure 1, the emissions except for a few emissions in Case 1 and emissions with wave frequencies f higher than 3.4 kHz in Case 3 propagate away from the equator.

Figure 2 shows the electric power spectral density of the upper hybrid resonance waves. In each panel of Figure 2, the arrow in red indicates the time of the strong upper-band chorus emissions shown in the corresponding case of Figure 1. Based on *Kurth et al.* [2015], we infer the cold plasma frequencies f_p and densities n of electrons from the upper hybrid resonance waves, and list them in Table 1. From Figure 2 and Table 1, we note that the upper-band chorus emissions for Case 1 were generated just inside the plasmapause. The emissions for Cases 2 and 3, on the other hand, occurred outside the plasmasphere.

According to the nonlinear wave growth theory [*Omura et al.*, 2008; *Omura and Nunn*, 2011], the whistler mode chorus elements are generated with parallel propagation ($\theta = 0°$). As shown in Figure 1b, the emissions in Cases 1 and 2 propagate quasi-parallel to the geomagnetic field line. From theoretical and Ray-tracing simulation results, respectively

shown in Figure 1 of *Hsieh and Omura* [2017] and Figure 3 of *Yamaguchi et al.* [2013], upper-band chorus emissions become oblique rapidly. Based on hybrid-code and full-particle simulations [e.g., *Katoh and Omura*, 2013; *Hikishima et al.*, 2010], the waves occur near the equator, not at the equator: i.e. the wave generation region has a certain range in latitudinal direction. Consequently, the waves in Case 3 could had been observed after moving further than 1.5° in latitude. Namely, the wave normal angles in Case 3 are possible to deviate from the parallel direction through propagation because of the curvature of the geomagnetic field. At the generation of each emission, the wave number $\boldsymbol{k}$ parallel to the geomagnetic field $\boldsymbol{B_0}$ is calculated based on the cold plasma dispersion relation [e.g., *Stix*, 1992] for a whistler mode wave, which is given for $\theta = 0°$ by

$$c^2k^2 = \omega^2 + \frac{\omega\omega_p^2}{\Omega_c - \omega} \ , \tag{1}$$

where $\omega_p = 2\pi f_p$ is the angular plasma frequency of electrons, and c, $\omega = 2\pi f$, and $\Omega_c = 2\pi f_c$ are the speed of light, the angular wave frequency, and the angular cyclotron frequency of an electron. When an electron is in cyclotron resonance with a whistler mode chorus wave, the resonance velocity V_R parallel to $\boldsymbol{B_0}$ can be expressed by the following non-relativistic first-order resonance condition:

$$V_R = \frac{\omega - \Omega_c}{k} \ . \tag{2}$$

Assuming $\omega = 0.5\Omega_c$ and substituting (2) into (1), we obtain the following equation:

$$\left(\frac{\omega_p}{\Omega_c}\right)^2 = \frac{1}{4}\left(\frac{c^2}{V_R^2} - 1\right) \ . \tag{3}$$

If a parallel velocity $v_\parallel$ of an electron is equal to the resonance velocity V_R, V_R can be expressed by $v\cos\alpha$, where v and α are the velocity and pitch angle of the electron. The resonance condition as a function of the ratio of the plasma frequency f_p to the cyclotron

frequency f_c is given by

$$v\cos\alpha = \frac{c}{\sqrt{4\left(f_p/f_c\right)^2 + 1}} \quad . \tag{4}$$

We calculate, for a whistler-mode wave with $\omega = 0.5\Omega_c$ and $\theta = 0°$, the pitch angles satisfying the resonance condition at kinetic energies K = 0.1, 0.5, 1, 5, 10, 50 keV, and plot them in Figure 3. The energy transfer from the electron to the wave is proportional to the perpendicular velocity $v_\perp = v\sin\alpha$ because the wave electric field is in the perpendicular direction. Therefore, the electrons with pitch angles far away from 0° excite the waves efficiently. According to Figure 3, the waves generated in a higher-density region ($f_p/f_c \sim 20$) can be resonant with electrons at energies even lower than 1 keV, while the waves occurring in a low-density region ($f_p/f_c < 5$) can be resonant with electrons at energies higher than 10 keV.

3. HOPE Observational Results

Using the HOPE data just before or in the midst of the generation of the emissions shown in Figure 1, we plot the pitch angle distributions of source electrons exciting these emissions in Figure 4a [*Funsten et al.*, 2013]. The HOPE instrument inherently measures 72 energy steps, however, early in the mission before data compression was enabled, HOPE was only able to report 36 energies because of mission telemetry constraints. The instrument then summed counts at pairs of adjacent energies on board and thus transmitted effectively only 36 channels. The ground software then evenly divided the summed counts back between the channels. That will result in the pairs of adjacent channels having closely similar phase space density. The smaller energy from each pair is plotted with a solid line, and the higher energy is plotted with a dashed line.

Figure 4b shows the resonance pitch angles satisfying $v_{\parallel} = V_R$ of electrons as a function of kinetic energy K. The black solid and dashed lines correspond to the minimum and maximum frequencies of the large amplitude chorus emissions shown in Figure 1. As indicated by the directions of the Poynting vectors shown in Figure 1c, the large amplitude elements in Cases 1 and 2 respectively propagate parallel and antiparallel to $\boldsymbol{B_0}$. In Case 3, on the other hand, two different groups of chorus elements overlap. Because the group propagating antiparallel to $\boldsymbol{B_0}$ consists of a wider range of rising-tone frequencies, we focus only on this group. We also plot the resonance condition for half the cyclotron frequency by a black dash-dotted line in each case. As explained in the previous section, electrons with pitch angles $\alpha = 45^\circ \sim 135^\circ$ shown in Figure 4a contribute to the generation of the emissions dominantly. As the energy increases, the resonance pitch angle range between the black solid and dashed lines becomes narrower. Then, we estimate the minimum and maximum resonance energies, which correspond to the maximum and minimum wave frequencies respectively, from the intersections with the gray line at $\alpha = 45^\circ$ in each case of Figure 4b. Based on this method, we obtain the resonance energy ranges $\Delta K_R =$ 5.82-246 eV, 0.98-14.4 keV, and 2.16-23.1 keV for Cases 1-3, respectively.

To estimate the parallel and perpendicular components of the thermal velocity ($V_{t\parallel}$, $V_{t\perp}$) of the source electrons generating the chorus emissions shown in Figure 1, we assume that the velocity distribution function of the source electrons is represented by a bi-Maxwellian F given by

$$F(K,\alpha) = F_0 \exp\left(-\frac{v_{\parallel}^2}{2V_{t\parallel}^2} - \frac{v_{\perp}^2}{2V_{t\perp}^2}\right) = F_0 \exp\left(-\frac{K\cos^2\alpha}{mV_{t\parallel}^2} - \frac{K\sin^2\alpha}{mV_{t\perp}^2}\right) \quad , \qquad (5)$$

where m is the mass of an electron. We assume that F_0 and the thermal velocities are constant values in the resonance energy range ΔK_R of each case.

First, we evaluate the perpendicular thermal velocity $V_{t\perp}$ from the phase space density of electrons with pitch angles 90°. Substituting $\alpha = 90°$ into (5), we obtain the following equation:

$$\ln F(K, 90°) = \ln F_0 - \frac{K}{mV_{t\perp}^2} \quad . \tag{6}$$

Using measured phase space densities F at $\alpha = 90°$ from Figure 4a, we calculate the LHS of (6) in the resonance energy ranges ΔK_R of 5.82-246 eV, 0.98-14.4 keV, and 2.16-23.1 keV for Cases 1-3, and plot them in Figure 5a. The red circles and black solid lines represent HOPE data and linear fits estimated from the observed phase space densities, respectively. We compute the perpendicular thermal velocity $V_{t\perp}$ from the slope of the fit corresponding to $1/(mV_{t\perp}^2)$ and list it in Table 1.

Using the perpendicular thermal velocity $V_{t\perp}$, we have introduced a new function $\tilde{F}$ given by

$$\tilde{F}(K, \alpha, V_{t\perp}) = \ln F(K, \alpha) + \frac{K \sin^2 \alpha}{mV_{t\perp}^2} \quad . \tag{7}$$

Substituting (5) into (7), we obtain

$$\tilde{F}(K, \alpha, V_{t\perp}) = \ln F_0 - \frac{v_\parallel^2}{2V_{t\parallel}^2} \quad . \tag{8}$$

We compute the LHS of (7) from the phase space densities F measured in the range of ΔK_R and $\alpha = 0 \sim 180°$. Using the calculated $\tilde{F}$, we obtain Figure 5b showing the relation between $\tilde{F}$ and $v_\parallel^2 = 2K \cos^2 \alpha / m$. Since the constant value F_0 and the parallel thermal velocity $V_{t\parallel}$ are part of the first and second terms of the RHS of (8), we evaluate them from the intercept and slope of the fitted line plotted in Figure 5b. They are listed in Table 1. The temperature anisotropies A defined as $A = V_{t\perp}^2/V_{t\parallel}^2 - 1$ of energetic electrons are 1.06 (Case 1), 0.35 (Case 2), and 0.53 (Case 3), respectively. From (4), the resonance velocity $V_R = v \cos \alpha$ depends on the plasma frequency f_p. As shown in Figure 3, the

electrons with lower energies can be resonant with the waves generated in a higher-density region. The chorus emissions for Case 1 (Cases 2 and 3) were generated inside (outside) the plasmapause as shown in Figure 2. Accordingly the thermal velocities ($V_{t\perp}, V_{t\parallel}$) for Case 1 are smaller than those for Cases 2 and 3.

Expressing a velocity vector $\boldsymbol{v}$ in terms of the absolute value $v = \sqrt{2K/m}$, pitch angle α, and gyro-phase ϕ, we can calculate the hot electron density n_h by

$$n_h = \iiint F d\boldsymbol{v} = \iiint F v^2 \sin\alpha dv d\alpha d\phi = \frac{2\sqrt{2}\pi}{m^{3/2}} \iint F\sqrt{K}\sin\alpha dK d\alpha \ , \qquad (9)$$

where $dv = dK/(mv) = dK/\sqrt{2mK}$. We integrate (9) over kinetic energy K between 5.82-246 eV, 0.98-14.4 keV, and 2.16-23.1 keV for Cases 1-3, respectively. With respect to the pitch angle α, we also integrate from 0 to π. The densities n_h of the hot electrons are listed in Table 1.

4. Comparison With the Linear and Nonlinear Wave Growth Theory

Setting up the parameters listed in Table 1, we obtain linear growth rates Γ_L computed by KUPDAP (Kyoto University Plasma Dispersion Analysis Package) [*Sugiyama et al.*, 2015] and plot them as red solid lines in Figure 6a. In KUPDAP, we choose a bi-Maxwellian distribution model for the source electrons. As shown in Figure 6a, Γ_L in Cases 2 and 3 are less than that of Case 1 ($\leq 2 \times 10^{-5}\Omega_c$). The initial amplitudes of the emissions are induced by the linear growth rates. However, Γ_L are too small (or negative) to explain the generation of the chorus emissions. Since the distributions shown in Figure 4a for Cases 2 and 3 are in the midst of the generation process of the emissions shown in Figure 1, the particles are observed after being scattered through the linear growth process. Therefore, it is difficult to evaluate Γ_L properly from the HOPE data.

Assuming that the frequency bandwidths of the chorus elements in Cases 1, 2, and 3 are respectively 205, 240, and 240 Hz, we select five chorus elements surrounded by the black squares shown in Figure 1a. In Case 3, we eliminate the power spectral densities of waves with the Poynting vectors $\theta_s < 90°$. In every time-window $\Delta t = 0.059$ s, we obtain a peak amplitude of a chorus element from a waveform given by inverse fast Fourier transform (IFFT) on a power spectral density. We plot the peak amplitudes $B_\perp$ perpendicular to the geomagnetic field $\boldsymbol{B_0}$ in Figure 6b. The wave amplitudes of Elements 1-5 shown in Figure 1a are plotted in either solid or dashed red lines in Figure 6b. The black vertical solid and dashed lines show the minimum and maximum frequencies of the large amplitude chorus emissions. The black dash-dotted lines represent half the cyclotron frequencies.

Assuming parallel propagation, *Omura et al.* [2009] and *Omura and Nunn* [2011] derived the threshold amplitude B_{th} and optimum amplitude B_{op} of chorus emissions generated through a nonlinear process, and they are respectively given by

$$B_{th} = 25\pi^3 \frac{mc^6 V_p s_2^2 V_{t\parallel}^2}{eQ^2\omega\omega_{ph}^4 V_{\perp 0}^5 \left(1 - V_p^2/c^2\right)^3} \left(\frac{\partial^2 \Omega_c}{\partial h^2}\right)^2 \exp\left(\frac{V_R^2}{V_{t\parallel}^2}\right) \quad , \tag{10}$$

and

$$B_{op} = 0.81\pi^{-5/2} \frac{mQ\omega_{ph}^2 V_{\perp 0} V_p V_g}{ec^2\omega\tau V_{t\parallel}} \left(1 - \frac{V_R}{V_g}\right)^2 \exp\left(-\frac{V_R^2}{2V_{t\parallel}^2}\right) \quad , \tag{11}$$

where s_2 is the coefficient related to the gradient of the magnetic field for the constant electron density model given by

$$s_2 = \frac{\omega}{2\Omega_c} \frac{V_{\perp 0}^2}{V_p c} - \frac{V_R}{c} \left[1 + \frac{\Omega_c - \omega}{2(\Omega_c - \omega)} \left(1 - \frac{V_p^2}{c^2}\right)\right] \quad . \tag{12}$$

We assume that the Lorentz factor given by $\gamma = [1 - (v/c)^2]^{-1/2}$ is equal to unity and e is the charge of an electron. The phase velocity V_p and group velocity V_g are determined from the cold plasma dispersion relation given by (1), and ω_{ph} is the angular plasma frequency

of the hot electrons. The variable h is a distance from the magnetic equator along the dipole geomagnetic field line and τ is a parameter specifying the nonlinear transition time in terms of the nonlinear trapping period. Based on theoretical analyses of *Omura et al.* [2009] and *Summers et al.* [2012], we assume that the depth of an electron hole Q and the average perpendicular velocity $V_{\perp 0}$ of hot electrons are equal to 0.5 and $\sqrt{\pi/2}V_{t\perp}$, respectively. In setting up the parameters listed in Table 1, we calculate the threshold amplitude B_{th} and optimum amplitude B_{op} at the equator (i.e. $h = 0$), and respectively plot them in blue and black solid lines in Figure 6b. Based on theoretical, simulation, and observational analyses [*Omura and Nunn*, 2011; *Hikishima and Omura*, 2012; *Kurita et al.*, 2012], we assume $\tau = 0.25 - 1.0$. Consequently, we find that the optimum wave amplitudes for $\tau = 0.25 - 1.0$ are in good agreement with the observational peak amplitudes as shown in Figure 6b. When the optimum amplitude is larger than the threshold amplitude, the wave amplitude grows up to the optimum value. In Case 1, the condition ($B_{op} > B_{th}$) is satisfied only in the frequency range close to (or higher than) half the cyclotron frequency, while those in Cases 2 and 3 are satisfied in both frequency ranges lower and higher than half the cyclotron frequency. Consequently, the emissions in Case 1 consist of the upper band chorus only, while both upper- and lower-band chorus emissions are found in Cases 2 and 3. For Cases 2 and 3 of Figure 6b, we find chorus emissions each of which has a narrow gap at half the cyclotron frequency of electrons. They can be interpreted in terms of the nonlinear damping mechanism at half the cyclotron frequency f_c proposed by *Omura et al.* [2009].

We calculate the nonlinear growth rate Γ_{NL} expressed by the following equation [*Omura et al.*, 2009]:

$$\Gamma_{NL} = \frac{\mu_0 V_g}{2}\sqrt{\frac{8e^3 V_p\left(1 - V_p^2/c^2\right)}{m\omega B_w}}V_{\perp 0}^{5/2} QG \ , \tag{13}$$

where μ_0 is the vacuum permeability and G is the velocity distribution function averaged over perpendicular velocity at the resonance velocity V_R given by

$$G = \frac{n_h}{(2\pi)^{3/2} V_{t\parallel} V_{\perp 0}} \exp\left(-\frac{V_R^2}{2V_{t\parallel}^2}\right) \ . \tag{14}$$

Assuming B_w equal to both, B_{th} and B_{op} (for $\tau = 0.5$), we plot the nonlinear growth rates Γ_{NL} in blue and black lines in Figure 6a, respectively. When $B_{op} \leq B_{th}$, the waves cannot grow, and Γ_{NL} are plotted with dashed lines. We note that the nonlinear growth rates Γ_{NL} are large enough to explain the generation of the emissions.

5. Summary and Discussion

We analyzed the waveform data obtained from EMFSIS and found large amplitude upper-band chorus emissions observed both inside and outside the plasmasphere. Using HOPE data, we obtained the phase space density of hot electrons. Approximating the distribution function of the hot electrons by a bi-Maxwellian distribution function, we estimated the parameters for the source electrons to calculate both linear and nonlinear growth rates. Having to fit one constant $V_{t\perp}$ and one constant $V_{t\parallel}$ over the entire energy range of resonant electrons, the energy range ΔK_R must be limited to be able to make a straight line fit shown in Figure 5. To make a reasonable "guess" for the "possible" energy range of resonant electrons, we estimated the minimum and maximum resonance energies, which respectively correspond to the maximum and minimum wave frequencies of each chorus element, from the intersections at the pitch angle $\alpha = 45^\circ$ as shown in

Figure 4b. Based on (6), we estimated $V_{t\perp}$ from the measured phase space density F of the electrons with $\alpha = 90°$ (see Figure 5a). Substituting $V_{t\perp}$ into (7), we introduced a new function $\tilde{F}$. Based on (8), we estimated $V_{t\parallel}$ from $\tilde{F}$ with $\alpha = 0 \sim 180°$ (see Figure 5b). The density n_h of the source electrons is specified by integration of (9) over ΔK_R and $\alpha = 0 \sim 180°$.

In the present study, we calculated wave growth rates and both optimum and threshold amplitudes for the nonlinear growth, using the parameters for source electrons obtained through a series of the procedures explained above. We summarize our findings as follows:

1. The chorus emissions are explained by the nonlinear growth rates, while the linear growth rates are too small for wave generation.

2. The wave peak-amplitudes of the chorus elements are consistent with the optimum amplitudes obtained by the nonlinear growth theory.

3. The energy range of hot electrons exciting the chorus emissions varies significantly depending on the plasma density of the cold electrons.

Both parameter estimation and nonlinear growth model are based on the parallel propagation while some of the chorus elements propagate obliquely; e.g., the wave normal angle $\theta \sim 45°$ in Case 3 (see Figure 1). *Hsieh and Omura* [2017] and *Yamaguchi et al.* [2013] show the possibility that the waves become oblique rapidly after they are generated with parallel propagation. We need to evaluate the effect of the oblique propagation on the generation mechanism. A statistical analysis for upper-band chorus emissions is also left as a future study.

Acknowledgments. All RBSP-EMFISIS data used in this paper are available from http://emfisis.physics.uiowa.edu/. The research at University of Iowa was supported un-

der NASA prime contract NAS5-01072. All RBSP-ECT data are publicly available at the Web site http://www.RBSP-ect.lanl.gov/. Processing and analysis of the HOPE data was supported by Energetic Particle, Composition, and Thermal Plasma (RBSP-ECT) investigation funded under NASA's Prime contract no. NAS5-01072. This work was supported by MEXT/JSPS KAKENHI grants 16J11490 and 17H06140. The authors appreciate the reviewers for their useful comments.

References

Funsten H. O., R. M. Skoug, A. A. Guthrie, E. A. MacDonald, J. R. Baldonado, R. W. Harper, K. C. Henderson, K. H. Kihara, J. E. Lake, B. A. Larsen, A. D. Puckett, V. J. Vigil, R. H. Friedel, M. G. Henderson, J. T. Niehof, G. D. Reeves, M. F. Thomsen, J. J. Hanley, D. E. George, J.-M. Jahn, S. Cortinas, A. DeLos Santos, G. Dunn, E. Edlund, M. Ferris, M. Freeman, M. Maple, C. Nunez, T. Taylor, W. Toczynski, C. Urdiales, H. E. Spence, J. A. Cravens, L. L. Suther, J. Chen (2013), Helium, Oxygen, Proton, and Electron (HOPE) Mass Spectrometer for the Radiation Belt Storm Probes Mission, *Space Sci. Rev. 179,* 423-484, doi:10.1007/s11214-013-9968-7.

Habagishi, H., S. Yagitani, and Y. Omura (2014), Nonlinear damping of chorus emissions at local half cyclotron frequencies observed by Geotail at L > 9, *J. Geophys. Res. Space Physics, 119,* 475-4483, doi:10.1002/2013JA019696.

Hsieh, Y.-K., and Y. Omura (2017), Nonlinear dynamics of electrons interacting with oblique whistler mode chorus in the magnetosphere, *J. Geophys. Res. Space Physics, 122,* 675-694, doi:10.1002/2016JA023255.

Hikishima, M., Y. Omura, and D. Summers (2010), Self-consistent particle simulation of whistler mode triggered emissions, *J. Geophys. Res.,* 115, A12246, doi:10.1029/2010JA015860.

Hikishima, M., and Y. Omura (2012), Particle simulations of whistler-mode rising-tone emissions triggered by waves with different amplitudes, *J. Geophys. Res., 117,* A04226, doi:10.1029/2011JA017428.

Katoh, Y., and Y. Omura (2013), Effect of the background magnetic field inhomogeneity on generation processes of whistler-mode chorus and broadband hiss-like emissions, *J. Geophys. Res. Space Physics, 118,* doi:10.1002/jgra.50395.

Kletzing C. A., W. S. Kurth, M. Acuna, R. J. MacDowall, R. B. Torbert, T. Averkamp, D. Bodet, S. R. Bounds, M. Chutter, J. Connerney, D. Crawford, J. S. Dolan, R. Dvorsky, G. B. Hospodarsky, J. Howard, V. Jordanova, R. A. Johnson, D. L. Kirchner, B. Mokrzycki, G. Needell, J. Odom, D. Mark, R. Pfaff Jr., J. R. Phillips, C. W. Piker, S. L. Remington, D. Rowland, O. Santolik, R. Schnurr, D. Sheppard, C. W. Smith, R. M. Thorne, and J. Tyler (2013), The Electric and Magnetic Field Instrument Suite and Integrated Science (EMFISIS) on RBSP, *Space Sci. Rev. 179,* 127-181, doi:10.1007/s11214-013-9993-6.

Kubota, Y., and Y. Omura (2017), Rapid precipitation of radiation belt electrons induced by EMIC rising tone emissions localized in longitude inside and outside the plasmapause, *J. Geophys. Res. Space Physics, 122,* 293-309, doi:10.1002/2016JA023267.

Kurita, S., Y. Katoh, Y. Omura, V. Angelopoulos, C. M. Cully, O. Le Contel, and H. Misawa (2012), THEMIS observation of chorus elements without a gap at half the gyrofrequency, *J. Geophys. Res., 117,* A11223, doi:10.1029/2012JA018076.

Kurth, W. S., S. De Pasciale, J. B. Faden, C. A. Kletzing, G. B. Hospodarsky, S. Thaller, and J. R. Wygant (2015), Electron densities inferred from plasma wave spectra obtained by the Waves instrument on Van Allen Probes, *J. Geophys. Res. Space Physics, 120*, 904-914, doi:10.1002/2014JA020857.

Li, W., J. Bortnik, R. M. Thorne, and V. Angelopoulos (2011), Global distribution of wave amplitudes and wave normalangles of chorus waves using THEMIS wave observations, *J. Geophys. Res., 116,* A12205, doi:10.1029/2011JA017035.

Mourenas, D., A. V. Artemyev, O.V. Agapitov, V. Krasnoselskikh, andF. S. Mozer (2015), Very oblique whistler generation by low-energyelectron streams, *J. Geophys. Res Space Physics, 120*, 3665-3683, doi:10.1002/2015JA021135.

Omura, Y., Y. Katoh, and D. Summers (2008), Theory and simulation of the generation of whistler-mode chorus, J. Geophys. Res., 113, A04223, doi:10.1029/2007JA012622.

Omura, Y., M. Hikishima, Y. Katoh, D. Summers, and S. Yagitani (2009), Nonlinear mechanisms of lower-band and upper-band VLF chorus emissions in the magnetosphere, *J. Geophys. Res., 114,* A07217, doi:10.1029/2009JA014206.

Omura, Y., and D. Nunn (2011), Triggering process of whistler mode chorus emissions in the magnetosphere, *J. Geophys. Res., 116,* A05205, doi:10.1029/2010JA016280.

Omura, Y., Y. Miyashita, M. Yoshikawa, D. Summers, M. Hikishima, Y. Ebihara, and Y. Kubota (2015), Formation process of relativistic electron flux through interaction with chorus emissions in the Earth's inner magnetosphere, *J. Geophys. Res. Space Physics, 120,* 9545-9562, doi:10.1002/2015JA021563.

Samson, J. C., and J. V. Olson (1980), Some comments on the descriptions of the polarization states of waves, *Geophys. J. R. Astron. Soc., 61*(1), 115-129.

Santolik, O., D. A. Gurnett, J. S. Pickett, J. Chum, and N. Cornilleau-Wehrlin (2009), Oblique propagation of whistlermode waves in the chorus source region, *J. Geophys. Res., 114*, A00F03, doi:10.1029/2009JA014586.

Santolik, O., C. A. Kletzing, W. S. Kurth, G. B.Hospodarsky, and S. R. Bounds (2014), Finestructure of large-amplitude chorus wavepackets, *Geophys. Res. Lett., 41,* 293-299, doi:10.1002/2013GL058889.

Stix, T. H. (1992), Waves in Plasmas, American Institute of Physics, New York.

Sugiyama, H., S. Singh, Y. Omura, M. Shoji, D. Nunn, and D. Summers (2015), Electromagnetic ion cyclotronwaves in the Earth's magneto-sphere with a kappa-Maxwellianparticle distribution, *J. Geophys. Res. Space Physics, 120,* 8426-8439, doi:10.1002/2015JA021346.

Summers, D., Y. Omura, Y. Miyashita, and D.-H. Lee (2012), Nonlinear spatiotemporal evolution of whistler mode chorus waves in Earth's inner magnetosphere, *J. Geophys. Res., 117*, A09206, doi:10.1029/2012JA017842.

Yagitani, S., T. Habagishi, and Y. Omura (2014), Geotail observation of upper band and lower band chorus elements in the outer magnetosphere, *J. Geophys. Res. Space Physics, 119,* 4694-4705, doi:10.1002/2013JA019678.

Yamaguchi, K., T. Matsumuro, Y. Omura, and D. Nunn (2013), Ray tracing of whistler-mode chorus elements: implications for generation mechanisms of rising and falling tone emissions *Annales Geophysicae, 31*(4), 665-673, doi:10.5194/angeo-31-665-2013.

Table 1. Parameters

Parameter	Case 1	Case 2	Case 3
L-value	5.57	4.70	5.18
Electron cyclotron frequency f_c	4.385 kHz	6.722 kHz	4.967 kHz
Magnitude of $\boldsymbol{B_0}$	156.65 nT	240.12 nT	177.45 nT
Electron plasma frequency f_p	22.8 f_c	3.75 f_c	3.26 f_c
Cold electron density n	124 /cc	7.89 /cc	3.26 /cc
$V_{t\perp}$ of hot electrons	0.0125 c	0.0802 c	0.0927 c
$V_{t\parallel}$ of hot electrons	0.0087 c	0.0692 c	0.0751 c
F_0 of hot electrons	1.43 $\times 10^{-15}\,\mathrm{s}^3/\mathrm{m}^6$	1.36 $\times 10^{-18}\,\mathrm{s}^3/\mathrm{m}^6$	8.42 $\times 10^{-19}\,\mathrm{s}^3/\mathrm{m}^6$
Hot electron density n_h	0.749 /cc	0.221 /cc	0.176 /cc

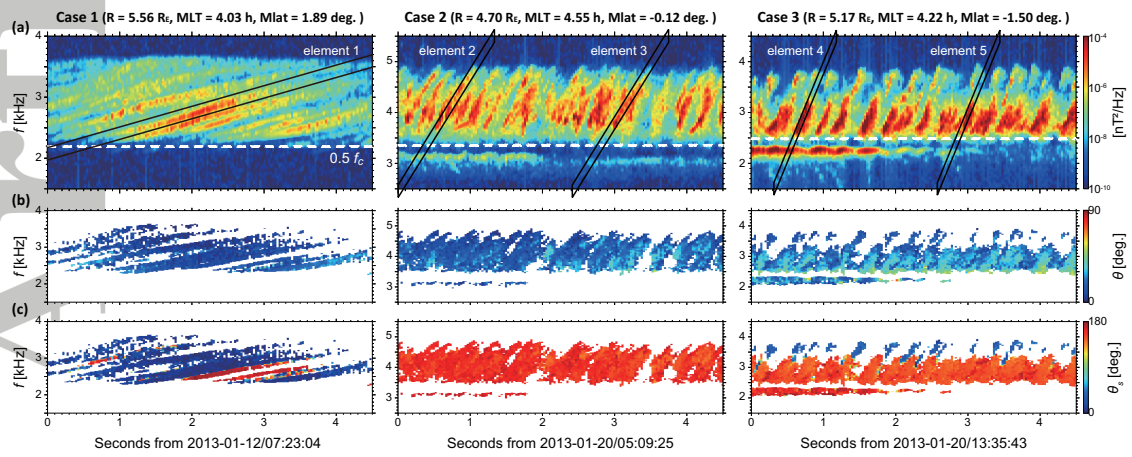

Figure 1. The upper-band chorus emissions of RBSP-A EMFISIS for Case 1 from 7:23:04.0 to 7:23:08.5 UT on 12 January 2013, Case 2 from 5:09:25.0 to 5:09:29.5 UT on 20 January 2013, and Case 3 from 13:35:43.0 to 13:35:47.5 UT on 20 January 2013. (a) The sum of magnetic power spectral densities of the two components perpendicular to the geomagnetic field $\boldsymbol{B_0}$, (b) the wave normal angle θ, and (c) the Poynting vector angle θ_s with respect to the geomagnetic field. Spectra in (b) and (c) are plotted only when the magnetic power spectral density and the degree of polarization are respectively greater than $10^{-7}\,\mathrm{nT}^2/\mathrm{Hz}$ and 0.7. The white dashed lines plotted in (a) represent half the local electron cyclotron frequencies f_c.

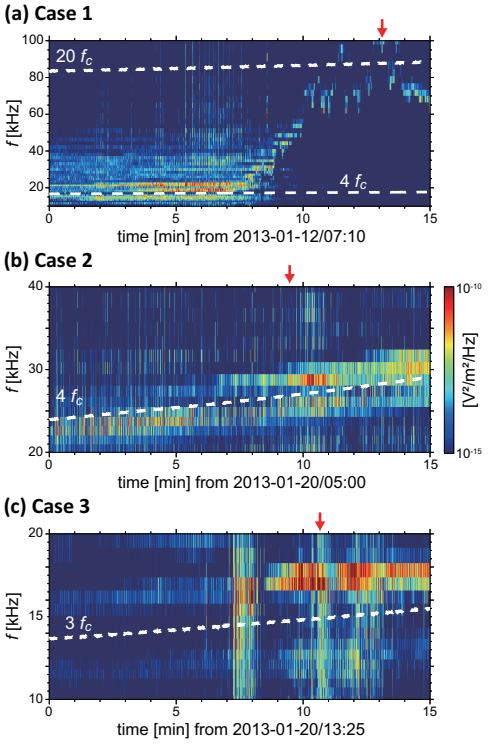

Figure 2. The electric power spectral density of the upper hybrid resonance waves obtained by RBSP-A EMFISIS for (a) Case 1 from 7:10 to 7:25 UT on 12 January 2013, (b) Case 2 from 5:00 to 5:15 UT on 20 January 2013, and (c) Case 3 from 13:25 to 13:40 UT on 20 January 2013. An arrow in red indicates the timing of observation of each case of the upper-band chorus emissions shown in Figure 1.

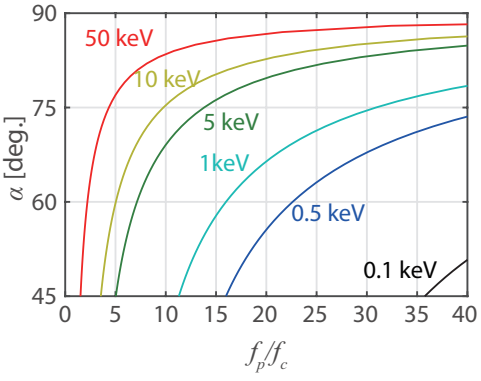

Figure 3. The pitch angles α of electrons satisfying the cyclotron resonance condition with a chorus wave at $\theta = 0°$ and $f \sim 0.5 f_c$ as a function of f_p/f_c.

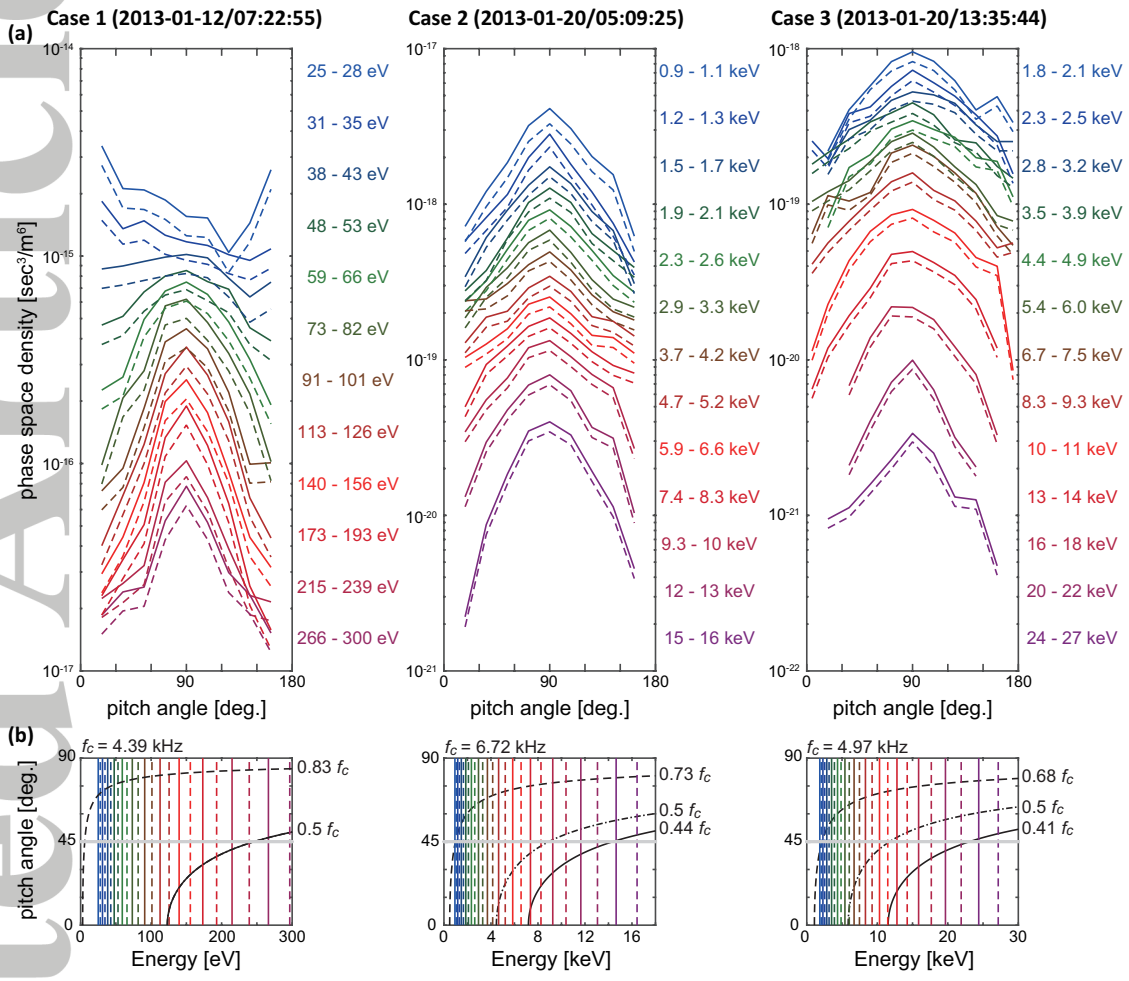

Figure 4. (a) Electron pitch angle distribution measured by RBSP-A HOPE for Case 1 (7:22:55 UT on 12 January 2013), Case 2 (5:09:25 UT on 20 January 2013), and Case 3 (13:35:44 UT on 20 January 2013). (b) The pitch angle of an electron with parallel velocity $v_{\parallel}$ equal to the cyclotron resonance velocity V_R as a function of its kinetic energy K. The black solid and dashed lines correspond to the minimum and maximum frequencies of the chorus emissions propagating away from the equator as shown in Figure 1. The vertical lines with different colors shown in (b) represent the kinetic energies of electrons plotted in the same color line shown in (a).

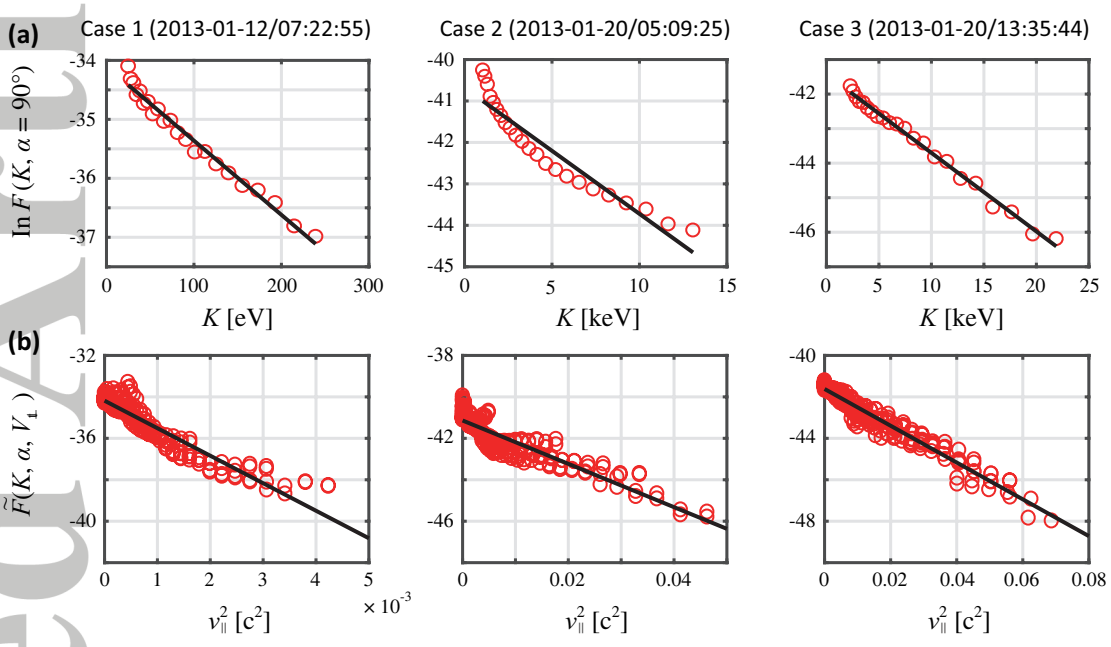

Figure 5. (a) The natural logarithm of phase space densities F of resonant electrons with pitch angles α equal to 90° as a function of the kinetic energy K. (b) The functions $\tilde{F}$ with respect to the square of electron parallel velocity $v_{\parallel}$. The red circles indicate the data obtained by RBSP-A HOPE for Case 1 (7:22:55 UT on 12 January 2013), Case 2 (5:09:25 UT on 20 January 2013), and Case 3 (13:35:44 UT on 20 January 2013). The black solid lines indicate linear functions estimated by the least squares method.

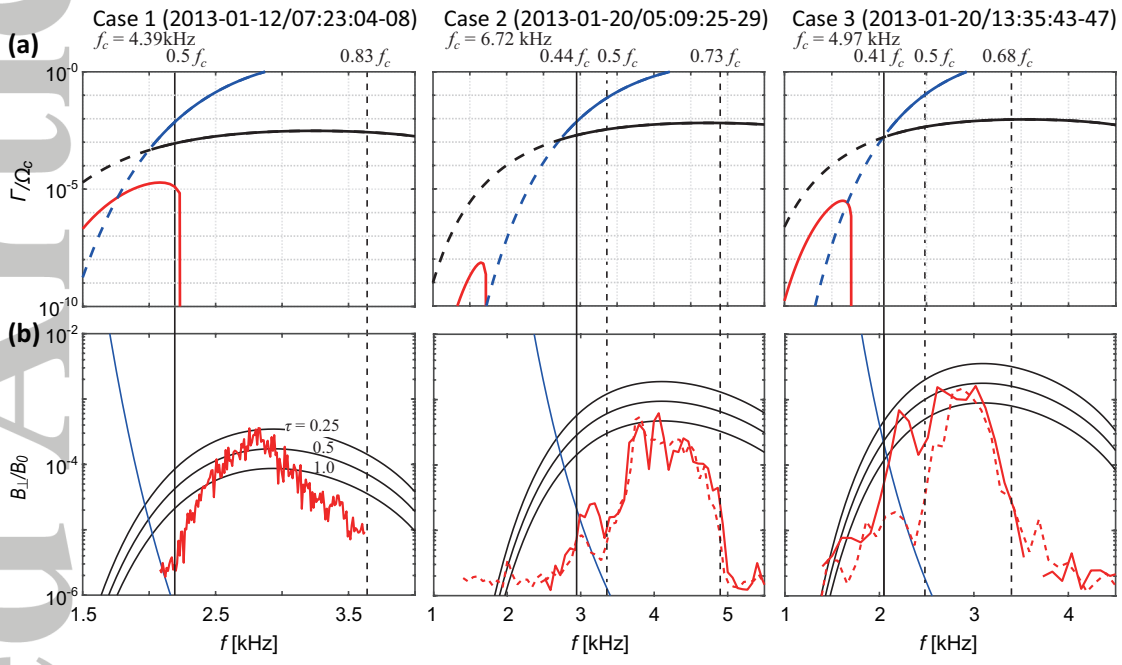

Figure 6. (a) Linear growth rates (in red), nonlinear growth rates for threshold amplitudes B_{th} (in blue), and nonlinear growth rates for optimum amplitudes B_{op} with τ= 0.5 (in black) as functions of wave frequency f. (b) The peak amplitudes $B_\perp$ perpendicular to the ambient magnetic field $\boldsymbol{B_0}$ for 5 chorus elements shown in Figure 1. The frequency ranges of chorus emissions are indicated by the solid and dashed vertical black lines. The blue and black lines represent the threshold and optimum wave amplitudes with different values τ for nonlinear wave growth [*Omura et al.*, 2009; *Omura and Nunn*, 2011].